Special Issue

Evaluating the Effects of Riboflavin/UV-A and Rose-Bengal/Green Light Cross-Linking of the Rabbit Cornea by Noncontact Optical Coherence Elastography

Manmohan Singh,[1] Jiasong Li,[1] Zhaolong Han,[1] Srilatha Vantipalli,[2] Chih-Hao Liu,[1] Chen Wu,[1] Raksha Raghunathan,[1] Salavat R. Aglyamov,[3] Michael D. Twa,[4] and Kirill V. Larin[1,5]

[1]Department of Biomedical Engineering, University of Houston, Houston, Texas, United States
[2]College of Optometry, University of Houston, Houston, Texas, United States
[3]Department of Biomedical Engineering, University of Texas at Austin, Austin, Texas, United States
[4]School of Optometry, University of Alabama at Birmingham, Birmingham, Alabama, United States
[5]Interdisciplinary Laboratory of Biophotonics, Tomsk State University, Tomsk, Russia

Correspondence: Michael D. Twa, School of Optometry, University of Alabama at Birmingham, HPB 515, 1716 University Boulevard, Birmingham, AL 35294-0010, USA; mtwa@uab.edu.
Kirill V. Larin, Department of Biomedical Engineering, University of Houston, 3605 Cullen Boulevard, Room 2028, Houston, TX 77204-5060, USA; klarin@uh.edu.

MS, JL, and ZH contributed equally to the work presented here and should therefore be regarded as equivalent authors.
MDT and KVL are joint senior authors.

Submitted: December 13, 2015
Accepted: March 4, 2016

Citation: Singh M, Li J, Han Z, et al. Evaluating the effects of riboflavin/UV-A and rose-Bengal/green light cross-linking of the rabbit cornea by noncontact optical coherence elastography. *Invest Ophthalmol Vis Sci*. 2016;57:OCT112–OCT120. DOI:10.1167/iovs.15-18888

Purpose. The purpose of this study was to use noncontact optical coherence elastography (OCE) to evaluate and compare changes in biomechanical properties that occurred in rabbit cornea in situ after corneal collagen cross-linking by either of two techniques: ultraviolet-A (UV-A)/riboflavin or rose-Bengal/green light.

Methods. Low-amplitude ($\leq$10 μm) elastic waves were induced in mature rabbit corneas by a focused air pulse. Elastic wave propagation was imaged by a phase-stabilized swept source OCE (PhS-SSOCE) system. Corneas were then cross-linked by either of two methods: UV-A/riboflavin (UV-CXL) or rose-Bengal/green light (RGX). Phase velocities of the elastic waves were fitted to a previously developed modified Rayleigh-Lamb frequency equation to obtain the viscoelasticity of the corneas before and after the cross-linking treatments. Micro-scale depth-resolved phase velocity distribution revealed the depth-wise heterogeneity of both cross-linking techniques.

Results. Under standard treatment settings, UV-CXL significantly increased the stiffness of the corneas by ~47% ($P < 0.05$), but RGX did not produce statistically significant increases. The shear viscosities were unaffected by either cross-linking technique. The depth-wise phase velocities showed that UV-CXL affected the anterior ~34% of the corneas, whereas RGX affected only the anterior ~16% of the corneas.

Conclusions. UV-CXL significantly strengthens the cornea, whereas RGX does not, and the effects of cross-linking by UV-CXL reach deeper into the cornea than cross-linking effects of RGX under similar conditions.

Keywords: corneal biomechanics, cross-linking, optical coherence elastography

The biomechanical properties of the cornea are inherently tied to its health,[1] consequently any changes in the biomechanical properties of the cornea can affect vision quality. Keratoconus is a structurally degenerative disease that can pathologically diminish visual acuity because the cornea thins and forms a conical shape due to a significant reduction in its stiffness.[2–4] Riboflavin/ultraviolet-A corneal collagen cross-linking (UV-CXL) is an emerging clinical treatment which increases the stiffness of the cornea and improves its ability to resist further degeneration.[5] Although UV-CXL has shown great promise,[6–8] there are concerns associated with UV irradiation, such as keratocyte cytotoxicity.[9–12] In addition, endothelial toxicity restricts the use of UV-CXL for corneas thinner than 400 μm.[12] Other side effects of UV-CXL have been reported, such as corneal haze,[13] keratitis and corneal scarring,[14] and endothelial cytotoxicity, even when the cornea was of sufficient thickness.[15] Nevertheless, these side effects are rare, and UV-CXL is gaining momentum as a treatment for keratoconus[6,8,16] and other conditions such as infectious keratitis.[17,18]

Rose-Bengal/green light corneal collagen cross-linking (RGX) has been proposed as an alternative to UV-CXL.[19] Because green light is used in lieu of UV irradiation, there is no or only minimal cytotoxicity.[19] Moreover, the high absorbance of green light by rose-Bengal dye results in a significantly shorter treatment time than with UV-CXL (30 min for RGX vs. 1 h for UV-CXL).

Currently, UV-CXL treatment has not been individualized to specific cases, and RGX has only recently been investigated as a corneal collagen cross-linking technique. If changes in the biomechanical properties of the cornea due to cross-linking could be accurately assessed, the treatment could be personalized to increase its efficacy and reduce the risk of side effects.

Investigative Ophthalmology & Visual Science

Therefore, a noninvasive technique which can quantitatively characterize the biomechanical properties of the cornea accurately would provide valuable insight into corneal biomechanical changes induced by cross-linking.

Several techniques have been proposed to assess biomechanical properties of the cornea. Commercial devices such as the Ocular Response Analyzer (ORA; Reichert Technologies, Buffalo, NY, USA) and CorVis ST (Oculus Optikgeräte GmbH, Wetzlar, Germany) have been able to detect differences between elasticity of the healthy corneas and that of keratoconic corneas[20–22]; however, there have been conflicting reports of their ability to detect changes in the stiffness of the cornea after UV-CXL.[20,23–25] Mechanical assessments by extensiometry[26] and inflation testing[27] have demonstrated how UV-CXL stiffens the cornea, but these techniques are inherently unfeasible for in vivo investigations. Acoustic techniques have also been used to assess the changes in elasticity after UV-CXL of ex vivo canine[28] and in vivo porcine corneas.[29] However, acoustic techniques require contact with the cornea and use of a transmission medium, such as water or gel, which may not be appropriate for clinical applications.

Brillouin microscopy is a noninvasive optical imaging technique which can provide a depth-resolved map of the Brillouin frequency shift in the cornea.[30,31] Brillouin microscopy has mapped the Brillouin shift of human corneas in vivo,[32] revealed differences in the Brillouin shift between healthy and keratoconic human corneal buttons ex vivo,[33] illustrated the depth-resolved effects of UV-CXL on the Brillouin shift of ex vivo porcine corneas,[34] and shown depth-resolved changes in the Brillouin shift induced by RGX on ex vivo rabbit corneas.[19] Although it is understood that the Brillouin shift may be related to elasticity, accurately obtaining quantitative biomechanical parameters (e.g., Young's modulus and viscosity) from the Brillouin shift is still a challenge.

Elastography is an established technique for quantitatively obtaining biomechanical properties of tissue by using an imaging modality to detect displacements. Traditional elastographic techniques such as ultrasound elastography (USE)[35,36] and magnetic resonance elastography (MRE)[37,38] are clinically available tools for detecting diseases such as hepatic fibrosis[39] and breast cancer.[40] However, these techniques require relatively large displacement amplitudes and have poor spatial and temporal resolutions, which limit their use for small and thin samples such as ocular tissues.

Optical coherence tomography (OCT)-based elastography (OCE)[41] is a rapidly emerging technique for imaging mechanical contrast of tissues with micrometer-scale spatial resolution.[42,43] By analyzing the phase of the complex OCT signal, displacement sensitivity can reach nanometer scale.[44] Although the imaging depth of OCT is limited to a few millimeters in scattering media such as tissue, this is not an issue in corneal applications due to the optical transparency and relatively small thickness of the cornea. Hence, OCE is specifically suited for characterizing the biomechanical properties of the cornea.

Previous elastic wave-based OCE techniques have used the group velocity of an externally induced elastic wave to characterize elasticity of the cornea.[45–47] However, models which translate the group velocity to Young's modulus often do not account for the thickness of the cornea nor the fluid-solid interface between the aqueous humor and the posterior surface of the cornea. We recently showed that the group velocity changes as a function of thickness when all other parameters are equal, and therefore, the thickness should be taken into account when quantifying the biomechanical properties of the cornea.[48] Furthermore, group velocity-based assessments only provide information about the elasticity of the sample, which is not fully reflective of its biomechanical properties. Therefore, we have developed a robust model for reconstructing the viscoelasticity of the cornea by modifying the Rayleigh-Lamb frequency equation (RLFE) to incorporate the solid-fluid effect at the boundary between the corneal posterior surface and aqueous humor.[49] Moreover, spectral analysis can provide the depth-resolved micrometer-scale phase velocity distribution in the cornea, which has previously been used to reveal the elasticity differences in cornea layers.[50]

In this work, we present the first direct comparison of viscoelastic changes in the cornea induced by UV-CXL versus those by using RGX. A focused air pulse ($\leq$1 ms) induced a low-amplitude ($\leq$10 μm) elastic wave in rabbit corneas in the whole eye globe configuration at an artificially controlled IOP.[51] The viscoelasticity of rabbit corneas before and after UV-CXL and RGX were quantified by our previously developed modified RLFE.[49] In addition, the differences in depth-wise effects of the cross-linking treatments were revealed by depth-resolved micrometer-scale phase velocity distribution.[50]

Methods

Cornea Preparation

Mature rabbit eyes (>6 months old) were obtained fresh (Pel-Freeze Biologicals, Rogers, AR, USA) and shipped overnight on ice. Samples were separated into two groups for the cross-linking experiments (n = 4 samples for each group). Extraneous tissues such as muscles were removed from the eye globe before all experiments, and eyes were visually inspected to ensure no damage had incurred during transportation and preparation. All OCE measurements were completed within 24 h of enucleation. After OCE experiments using the virgin corneas were conducted, the cross-linking procedures were performed, and OCE measurements were repeated.

UV-CXL was performed according to our previous work, which mimicked the most commonly used clinical protocol.[5,6,52] Briefly, epithelium was removed, and a 0.1% riboflavin solution in 20% dextran was applied to the corneal surface every 5 min for 30 min. The cornea was then irradiated with UV-A (365 nm, 7-mm-diameter spot on the corneas, 3 mW/cm^2) for 30 min. During UV irradiation, the riboflavin solution was topically instilled every 5 min.

Rose-Bengal/green light was performed by applying a solution of 0.1% rose-Bengal dye in 0.9% phosphate-buffered saline every 5 min for 20 min after epithelium was removed. The cornea was then irradiated with green light (560 nm, 7-mm-diameter spot, 0.25 W/cm^2) for 10 min.[19]

Phase-Stabilized Swept Source Optical Coherence Elastography (PhS-SSOCE) System

Custom-built PhS-SSOCE system consisted of a phase-stabilized swept source optical coherence tomography system[53,54] and a focused air pulse delivery device.[51] The PhS-SSOCT system included a broadband SS laser (HSL2000; Santec, Inc., Hackensack, NJ, USA) with a central wavelength of ~1,310 nm, a bandwidth of ~130 nm, an A-scan rate of 30 kHz, an axial resolution of ~11 μm in air, and a phase stability of ~40 nm during the corneal experiments. The focused air pulse delivery device was composed of a controller and an electronically controlled pneumatic solenoid. The air pulse was expelled from an air port, which had a flat edge and an inner diameter of ~150 μm. The air source pressure was controlled by a standard pneumatic valve and monitored by a pressure gauge. The air pulse was positioned precisely with a three-dimensional (3D) linear micrometer stage, and the port was kept at ~400 μm from the surface of the corneas. To image the air pulse-induced elastic wave, successive (n = 501) M-

Investigative Ophthalmology & Visual Science

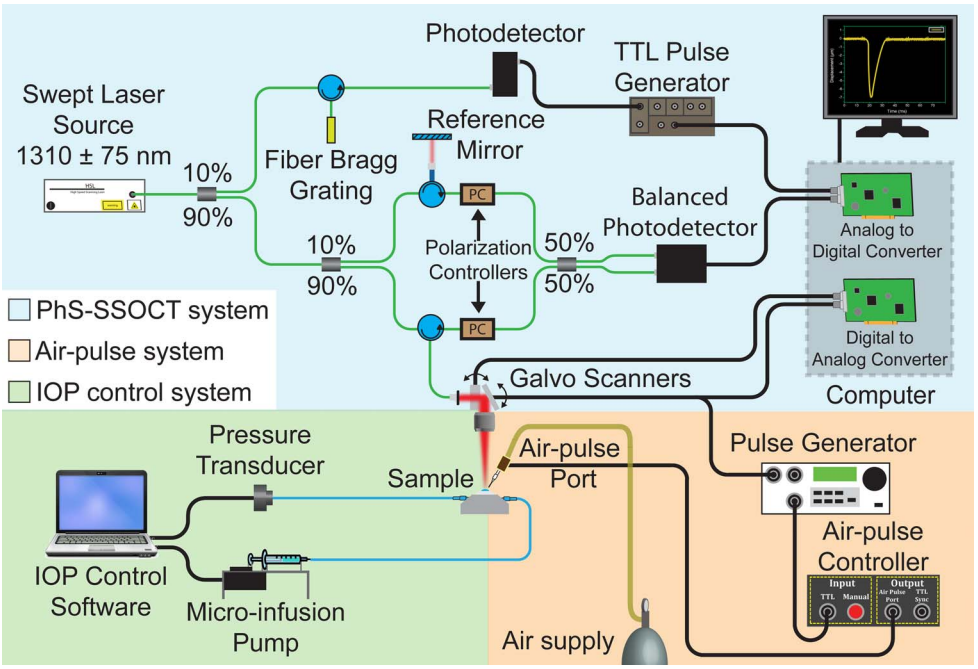

Figure 1. Optical coherence elastography experimental setup.

mode images were acquired in a line over ~6.3 mm (M-B mode), with the apex of the cornea at the middle of the scan. The air pulse excitation was also at the apex of the cornea. By synchronizing the M-mode frame trigger and air pulse with a transistor-transistor logic (TTL) signal, the PhS-SSOCT system effectively imaged the same elastic wave.[47]

In addition to the intrinsic corneal structure, IOP can have a significant effect on the measured elasticity of the cornea.[46,55] Therefore, the IOP of the eyes was artificially controlled by a homemade closed-loop IOP control system.[52] Whole rabbit eyes were placed in a customized holder, which had two holes for the IOP control system. Eye globes were cannulated with two 23-gauge needles: one needle was connected by tubing to a microinfusion pump, and the other needle was connected by tubing to a pressure transducer. A physiological IOP of 15 mm Hg was maintained during all experiments. A schematic representation of the experimental setup is illustrated in Figure 1.

The raw unwrapped vertical temporal phase profiles for the surface of the cornea, $\varphi_{surface}(t)$, were converted to displacement, $d_{surface}(t)$, by[56]

$$d_{surface}(t) = \varphi_{surface}(t) \times \frac{\lambda_0}{4\pi n_{air}} \quad (1)$$

and the raw unwrapped phase profiles within the cornea, $\varphi_{inside}(t)$, were translated to displacement, $d_{inside}(t)$, after correcting for the corneal surface motion and refractive index mismatch between air and the cornea by[47,57]

$$d_{inside}(t) = \left[\varphi_{inside}(t) + \varphi_{surface}(t) \times \frac{n_{cornea} - n_{air}}{n_{air}}\right] \times \frac{\lambda_0}{4\pi n_{cornea}} \quad (2)$$

where $n_{air} = 1$, $n_{cornea} = 1.376$,[58] and λ_0 was the central wavelength of the OCT system.

Phase Velocity

Phase velocities of the air pulse-induced elastic wave were used to quantify the viscoelasticity of the corneas and to obtain the depth-wise heterogeneity of the cross-linking techniques. For each in-depth layer, z, a fast Fourier transform was performed with the temporal displacement profile at each OCE measurement position, x, to obtain a phase shift, $\Delta\theta_{x,z,f}$, for each a fast Fourier transform bin frequency, f. The elastic wave propagation distance to each of the OCE measurement positions, Δr_x, incorporated the curvature of the cornea to ensure accuracy of the phase velocity calculations. The phase velocity for each in-depth layer and each bin frequency, $c_p(z, f)$, was calculated by linearly fitting the phase shifts to their corresponding propagation distances by $c_p(z, f) = 2\pi f \Delta r_x / \Delta\theta_{x,z,f}$.[50]

Viscoelasticity Reconstruction

Phase velocities were averaged depth-wise for each sample and fitted to our previously developed viscoelasticity reconstruction model based on a modified RLFE.[49] Briefly, the RLFE describes a symmetrical or antisymmetrical wave assuming free boundary conditions.[59] However, this does not account for the fluid-solid interface between the aqueous humor and posterior surface of the cornea. Therefore, the boundary condition at the corneal posterior surface was incorporated into the RLFE. The OCE-measured phase velocities were fitted to the analytical solution of the modified RLFE, and the viscoelasticity was determined by an iterative gradient-based procedure until the error between the OCE data and analytical solution was minimized. Figure 2 shows a typical fitting of the modified RLFE to OCE-measured phase velocities from a cornea before (Fig. 2a) and after (Fig. 2b) RGX.

Depth-Wise Effects of Cross-Linking

Depth-wise phase velocities were used to obtained the micrometer-scale depth-resolved elasticity of the cornea.[50] The turning point of the smoothed depth-wise phase profile (i.e., where $dc_p/dz = 0$, and z is depth) (Fig. 3a, blue arrow) was used to determine the region affected by the respective cross-linking techniques. The affected region (AR%) was determined by dividing the thickness of the cross-linked region

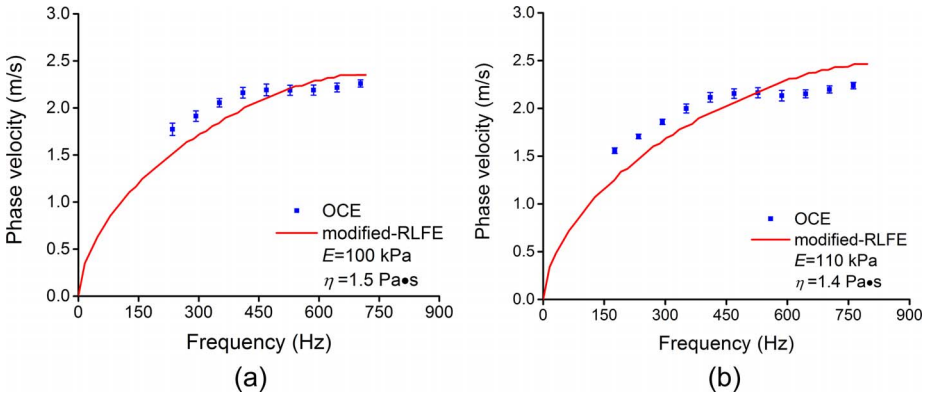

Figure 2. Fitting of the modified RLFE to the OCE measurements from a cornea (**a**) before and (**b**) after RGX to estimate Young's modulus, E, and shear viscosity, η.

(anterior surface of the cornea to the turning point) by the central corneal thickness (CCT) of the corresponding virgin cornea. To demonstrate that the posterior stroma was not affected by cross-linking treatments, the slopes of the phase velocity versus depth for corresponding posterior regions between the virgin and cross-linked corneas were compared and found to be nearly equal in all samples before and after the cross-linking treatments.

Results

Central Corneal Thickness

Central corneal thickness was calculated from the OCT structural image after correction for the refractive index of the cornea and is plotted in Figure 4. Before UV-CXL, the mean CCT of the corneas was 724 ± 135 μm, which decreased to 506 ± 67 μm after UV-CXL (change of ~30%). The CCT averages of the corneas before and after RGX were 754 ± 36 μm and 728 ± 41 μm, respectively (change of ~3%). Statistical analysis by a 1-tailed paired *t*-test showed that only the change in CCT after UV-CXL was significant ($P < 0.05$), which was primarily due to the topical instillation of dextran.

Viscoelasticity

The changes in viscoelasticity as quantified by the modified RLFE are plotted in Figure 5. Figure 5a shows that before UV-CXL, the average Young's modulus of the rabbit corneas was 73.0 ± 15.4 kPa, which increased to 107.5 ± 25.0 kPa after UV-CXL (change of ~47%). The mean elasticity values of the virgin and RGX-treated corneas were 79.0 ± 19.3 kPa and 80.0 ± 26.5 kPa, respectively (change of ~1%). Figure 5b shows that the shear viscosities of the corneas before and after UV-CXL were1.0 ± 0.3 Pa · s and 1.1 ± 0.3 Pa · s, respectively. The shear viscosity of the corneas before RGX was 1.0 ± 0.4 Pa · s and 1.0 ± 0.4 Pa · s after RGX. Only the change in stiffness after UV-CXL was significant ($P < 0.05$ by a 1-tailed paired *t*-test).

Results of Depth-Wise Effects of Cross-Linking

Figure 6 shows the mean affected region (AR%) of the corneas after each treatment. After UV-CXL, the anterior 34 ± 4% of the corneas was stiffened, and the anterior 16 ± 2% of the corneas was affected by the RGX treatment.

Discussion

We have used a noncontact OCE technique to compare the biomechanical changes in rabbit cornea induced by UV-CXL and RGX. By using a previously developed viscoelasticity reconstruction method based on a modified RLFE,[49] Young's modulus and shear viscosity values of the corneas before and after cross-linking using both techniques were quantified. Furthermore, the changes in the depth-resolved elastic wave phase velocities in the cornea after UV-CXL and RGX were compared to reveal the depth-wise heterogeneity of the cross-linking techniques. Our results show that the cornea is significantly stiffened by UV-CXL but not by RGX, and the

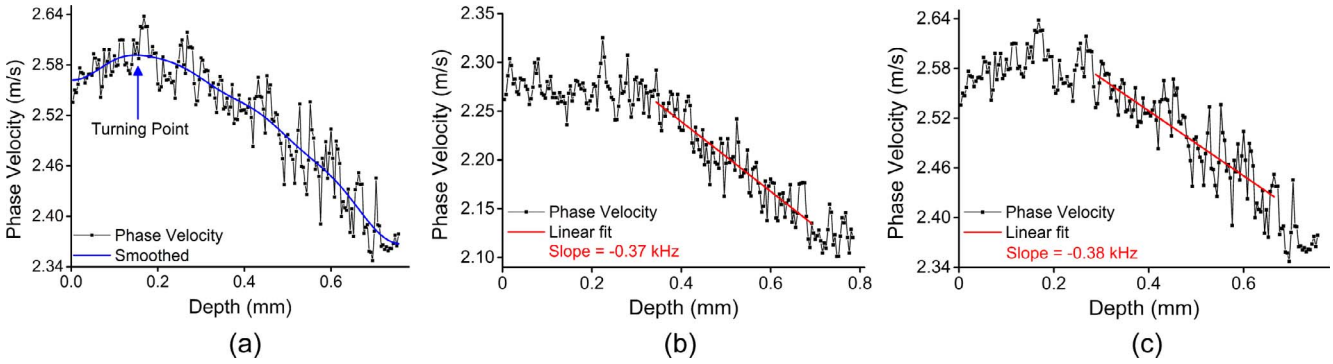

Figure 3. (**a**) Raw and smoothed depth-wise phase velocity distribution at 410 Hz showing the turning point (*blue arrow*) used to determine the cross-linking–affected region (AR%). Typical depth-wise phase velocity distribution before (**b**) and after (**c**) RGX from a selected sample, with the slope of the phase velocities in the posterior stroma.

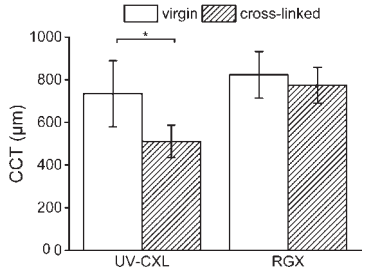

Figure 4. Change in CCT after both cross-linking techniques. *Statistical significance ($P < 0.05$), as calculated by a 1-tailed paired *t*-test. *Error bars* represent intersample standard deviations.

shear viscosities of the cornea were unaffected by either cross-linking technique. Furthermore, the effects of UV-CXL treatment penetrated deeper into the cornea as compared to the RGX treatment.

Statistical testing was performed to compare the parameters (CCT, Young's modulus, and shear viscosity) measured before and after cross-linking by using a 1-tailed paired *t*-test rather than a 2-tailed test to increase the power of the test (i.e., probability of not committing a type II error) because the expected direction of the change was known. For example, it is expected that the CCT will decrease after cross-linking, so a 1-tailed test is more powerful than a 2-tailed test.

For clinical application of this method, the acquisition time needs to be reduced. The acquisition time for each of 501 M-mode images was 100 ms, resulting in clinically unfeasible measurement times, and was exceeding the maximum permissible exposure (MPE) for the cornea. Moreover, the relatively large number of excitations may not be comfortable, even though the pressure on the corneal surface is relatively low (a few Pa).[51] Recently, we demonstrated a noncontact phase-sensitive OCE technique at ~1.5 million A-lines per second, where the air pulse-induced elastic wave was directly imaged by acquiring multiple B-scans (B-M mode) over the measurement region with a total acquisition time of ~30 ms.[60] The rapid scanning and acquisition would also reduce the influence of ocular motion, which would require complex signal processing techniques if in vivo OCE measurement were made with the technique in the presented work. When we used B-M mode acquisition, only a single excitation was necessary for a line measurement, whereas M-B mode imaging (as in the present work) requires an excitation for each OCE measurement position. Moreover, the reduced data size from B-M mode imaging meant that an elasticity estimate was given significantly more quickly. Rapid acquisition and B-M mode scanning ensured that the American National Standards Institute Standard for Safe Use of Lasers (ANSI Z136.1) maximum permissible exposure limit for the cornea was not surpassed, whereas the exposure limit was exceeded in this work. Coupled with a graphics processing acceleration unit,[61] parallel scanning and acquisition techniques,[62,63] and even faster OCT sources,[64] OCE may be able to provide elasticity assessments in near real time.

Previous investigations have used ORA,[24,25] CorVis ST,[20] extensiometry,[26] inflation testing,[27] Brillouin microscopy,[34] USE,[28,29] and OCE[65–67] to assess biomechanical properties of the cornea after UV-CXL. Although ORA and CorVis ST were unable to discern the effects of UV-CXL on the elasticity of the cornea, the other techniques were able to demonstrate how UV-CXL increases the stiffness of the cornea. Our results showed that UV-CXL increased the stiffness of the cornea by ~47%, which is similar to the ~59% increase in stiffness of in situ porcine corneas, measured by inflation tests[27] and the ~55% decrease in the tangential strain of in situ canine eyes as assessed by USE.[28] On the other hand, there is a wide variance in published reports of changes in elasticity of the cornea after UV-CXL. For example, strip extensiometry showed that Young's modulus of human, porcine, and rabbit corneas increased ~450%, ~180%, and ~850% after UV-CXL, respectively.[19,26] Our previous strip extensiometry results on rabbit corneas showed a ~73% increase in Young's modulus after UV-CXL[52] and that the elastic wave velocity in a porcine cornea at 15 mm Hg IOP increased ~80%, which would correspond to an increase in the stiffness of ~200%.[46] Supersonic shearwave imaging (SSI) indicated that Young's moduli of porcine corneas increased between 238% and 760% after UV-CXL.[29] This wide variation can be attributed to the different samples used (human, porcine, canine, and rabbit), the method used to assess the elasticity (mechanical, acoustic-based, and optical techniques), and the testing conditions (in vitro strips, in situ whole eye-globes, and in vivo). Furthermore, IOP has a significant effect on the measured elasticity of the cornea,[46,68,69] which is why IOP was controlled in this work.

The overall elasticity of the rabbit corneas increased ~1% after RGX, as assessed by the present technique, which was not statistically significant by a 1-tailed *t*-test, but extensiometry has shown that the stiffness of the rabbit cornea increased ~340% after RGX.[19] However, extensiometry cannot replicate the physiological conditions encountered in the whole eye globe configuration, and Young's moduli as assessed by OCE are a few orders of magnitude less than those measured by extensiometry.[26,45,49,52] It has been postulated that the equivalent IOP during extensiometry can be a few hundred millimeters of mercury.[70] Combined with the nonlinear stress-strain curve of the cornea, these two factors can explain the

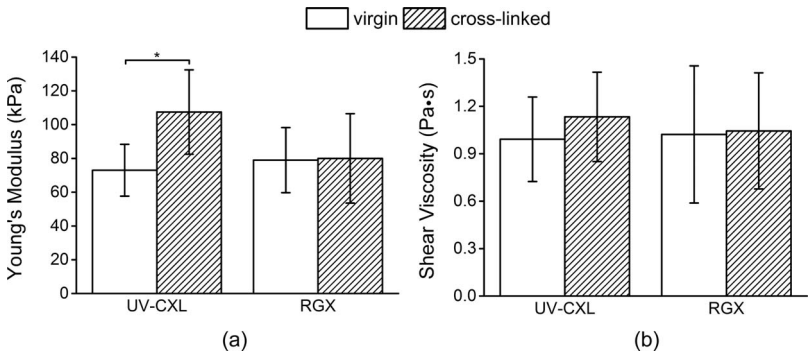

Figure 5. (**a**) Young's modulus and (**b**) shear viscosity as estimated by OCE-measured phase velocities fitted to the modified RLFE. *Statistical significance ($P < 0.05$, using a 1-tailed paired *t*-test). *Error bars* represent intersample standard deviations.

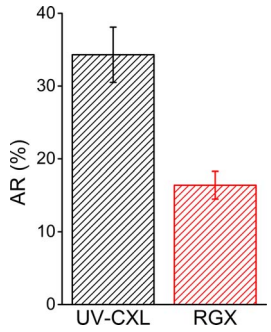

FIGURE 6. Affected region (AR%) of UV-CXL and RGX corneas. *Error bars* represent intersample standard deviations.

large discrepancy in Young's modulus between mechanical testing and our OCE measurements. We are currently investigating alternative techniques with which to obtain the biomechanical properties of the cornea in situ to validate our OCE measurements.

Results showed that the anterior ~1/3 of the cornea was stiffened by the UV-CXL treatment, which corroborates previous investigations using Brillouin microscopy[34] and USE.[28] The riboflavin solution is applied as a photosensitizer and UV shield. Hence, most UV absorption and subsequent cross-linking occurs in the anterior of the cornea where the riboflavin is present.[12] Slit-lamp illumination revealed a distinct demarcation at ~40% of the corneal thickness.[71] However, this line only became apparent 2 weeks after the treatment, and the elasticity assessments by Brillouin microscopy, USE, and OCE (including the present work), were performed immediately after the UV-CXL treatment was completed. Future investigations will assess the long-term depth-resolved elasticity changes in the cornea after UV-CXL.

The depth-resolved changes in the biomechanical properties of the cornea after RGX have been investigated by using Brillouin microscopy, which revealed that the anterior ~16% of the cornea was stiffened by RGX treatment.[19] Fluorescence analysis illustrated that most of the rose-Bengal dye penetrated only ~100 μm into the anterior stroma. Because cross-linking will occur predominantly where the green light is absorbed, due to the transparency of the cornea, these results are intuitively reasonable and similar to our findings. It has been hypothesized that electrostatic interactions between negatively charge rose-Bengal dye and positively charged amino acids in collagen trap the dye within the anterior stroma. Our future work will entail longer soak times to determine if this can increase the penetrative stiffening of RGX. The relatively small region of cross-linked tissue may also explain the insignificant increase in stiffness of the corneas after RGX. Because the modified RLFE provides the overall elasticity of the cornea, the small cross-linked region did not significantly contribute to an increase in the overall stiffness of the cornea. In addition, a decrease in the thickness of the sample would result in a smaller measured elasticity by the modified RLFE.[49] The relatively small cross-linked region combined with the decrease in thickness may explain why there was no measured increase in the overall stiffness of the corneas after RGX.

Viscosity is another important parameter to consider when assessing the biomechanical properties of the cornea, but it is hard to measure directly. In this work, the shear viscosity of the cornea was quantified by the modified RLFE, and the results showed no measurable differences in shear viscosity after cross-linking by either technique. This may be one reason that ORA and CorVis ST encounter difficulty when detecting changes in the biomechanical properties of the cornea after cross-linking, as their measurements are thought to be related primarily to the viscous damping ability of the cornea.[20,23–25]

In addition to the inherent microstructural changes in the cornea induced by the cross-linking treatments, the corneal thickness shrank ~30% and ~3% after UV-CXL and RGX, respectively. We have recently shown that the thickness and curvature, when all other parameters are fixed, can affect the elastic wave group velocity and subsequent elasticity assessment.[48] Although the group velocity was used to study the effects of the thickness and curvature, phase velocities are spectral decompositions of the group velocity and would similarly be affected by the changes in thickness and curvature. The modified RLFE was chosen to quantify the viscoelasticity of the cornea because it considers the thickness of the cornea. However, the modified RLFE assumes the sample is a flat thin plate, which is not strictly true of the cornea, and the curvature can affect the wave velocity.[48] Because the rabbit cornea is relatively small, the more significant curvature may be a source for the relatively poor fitting (Fig. 2) of the modified RLFE as compared to the porcine cornea.[49] This may result in inaccuracies when reconstructing the viscoelasticity of the cornea. In addition, the modified RLFE assumes the sample is a single isotropic homogenous layer, which also is not true of the cornea. Nevertheless, the modified RLFE performs accurately compared to mechanical testing.[49,72]

Depth-wise micrometer-scale phase velocity distribution can only reveal the layers of the cornea, it cannot provide a quantitative viscoelastic assessment of the corneal layers. The modified RLFE assumes the sample is a homogeneous and isotropic single-layer medium and therefore cannot be directly used to quantify the viscoelasticity of the individual layers of the cornea.[49,59,72] Development of a more robust mechanical model that can incorporate the layered, anisotropic, and curved geometry of the cornea to accurately quantify depth-resolved viscoelasticity is in progress.

There may be several sources for the relatively large viscoelastic inter-sample variance of the virgin corneas. The OCE measurements were taken only in one radial angle, and it has been shown that the cornea exhibits elastic anisotropy.[73–76] Therefore, imaging along different radial directions may increase intra-sample variance of the biomechanical properties. Future investigations will ensure that the elastic wave propagation is imaged along the same direction for all samples. We did, however, ensure that the OCE measurements were taken over the same region before and after cross-linking for a given sample to reduce intra-sample variability. Moreover, SSI showed that the elastic anisotropy becomes apparent only at relatively high IOPs (20 mm Hg),[75] whereas a physiological IOP of 15 mm Hg was maintained during all OCE measurements in this work. Currently, there has not been an investigation of the effects of cross-linking on the mechanical anisotropy of the cornea, and this is the future direction of our research. In addition to anisotropy, the age of the samples may have contributed to relatively large variations in viscoelasticity.[47,77,78] Nevertheless, all parameters assessed for the virgin corneas were not significantly different ($P > 0.05$ by a 2-tailed paired *t*-test for CCT, Young's modulus, and shear viscosity) between the two cross-linking groups.

Although UV-CXL has been proven to be an effective cross-linking technique in the clinic,[6,8,16] RGX has been proposed as an alternative to UV-CXL without harmful UV-A irradiation.[19] Brillouin microscopy and extensiometry showed that RGX increased the stiffness of the cornea by at least 3× without any keratocyte cytotoxicity. However, our results showed that Young's modulus of the whole cornea in the whole-eye globe configuration at 15 mm Hg IOP increased only ~1%, which was not statistically significant. Nevertheless, RGX may still be an

effective cross-linking treatment for corneas that may not be eligible for UV-CXL due to insufficient thickness or other complications. There is an extensive number of published reports of experimental and clinical investigations of UV-CXL, but RGX investigations are limited, and our results warrant further work.

Conclusions

We have presented a comparison between the viscoelastic changes in rabbit cornea after UV-CXL versus those after RGX by noncontact OCE. In addition, the depth-resolved micrometer-scale phase velocity distribution in the cornea after both of the cross-linking techniques was used to reveal the depth-wise heterogeneity after both of the cross-linking techniques. Results showed that UV-CXL significantly increased Young's modulus of the cornea by ~47% but that RGX did not significantly alter the stiffness of the cornea. The shear viscosities were unaffected by either of the cross-linking technique. Spectral analysis demonstrated that the UV-CXL treatment increased the stiffness of the anterior 1/3 of the cornea, whereas RGX predominantly affected the anterior 1/7 of the cornea. Because of noncontact excitation and imaging, OCE may be potentially useful for assessing the dynamic changes in biomechanical properties of the cornea before and after cross-linking in vivo.

Acknowledgments

The authors thank University of Houston undergraduate students Achuth Nair, Shezaan Noorani, Ericka Lafon, Thomas Hsu, Jayson VanMarter, and Chandni Kamdar for help with processing data and phantom experiments.

This study was funded, in part by National Institutes of Health grants 1R01EY022362, 1R01HL120140, and U54HG006348 and United States Department of Defense/Naval Sea Systems Command Grant PRJ71TN.

Disclosure: **M. Singh**, None; **J. Li**, None; **Z. Han**, None; **S. Vantipalli**, None; **C.-H. Liu**, None; **C. Wu**, None; **R. Raghunathan**, None; **S.R. Aglyamov**, None; **M.D. Twa**, None; **K.V. Larin**, None

References

1. Andreassen TT, Simonsen AH, Oxlund H. Biomechanical properties of keratoconus and normal corneas. *Exp Eye Res*. 1980;31:435–441.
2. Rabinowitz YS. Keratoconus. *Surv Ophthalmol*. 1998;42:297–319.
3. McGhee CN. Keratoconus: the arc of past, present and future. *Clin Exp Optom*. 2013;96:137–139.
4. Carney LG. Visual loss in keratoconus. *Arch Ophthalmol*. 1982;100:1282–1285.
5. Wollensak G, Spoerl E, Seiler T. Riboflavin/ultraviolet-a-induced collagen crosslinking for the treatment of keratoconus. *Am J Ophthalmol*. 2003;135:620–627.
6. O'Brart DP. Corneal collagen cross-linking: a review. *J Optom*. 2014;7:113–124.
7. Wittig-Silva C, Chan E, Islam FM, Wu T, Whiting M, Snibson GR. A randomized, controlled trial of corneal collagen cross-linking in progressive keratoconus: three-year results. *Ophthalmology*. 2014;121:812–821.
8. Meek KM, Hayes S. Corneal cross-linking–a review. *Ophthalmic Physiol Opt*. 2013;33:78–93.
9. Armstrong BK, Lin MP, Ford MR, et al. Biological and biomechanical responses to traditional epithelium-off and transepithelial riboflavin-UVA CXL techniques in rabbits. *J Refract Surg*. 2013;29:332–341.
10. Wollensak G, Spoerl E, Reber F, Seiler T. Keratocyte cytotoxicity of riboflavin/UVA-treatment in vitro. *Eye (Lond)*. 2004;18:718–722.
11. Wollensak G, Spoerl E, Wilsch M, Seiler T. Keratocyte apoptosis after corneal collagen cross-linking using riboflavin/UVA treatment. *Cornea*. 2004;23:43–49.
12. Spoerl E, Mrochen M, Sliney D, Trokel S, Seiler T. Safety of UVA-riboflavin cross-linking of the cornea. *Cornea*. 2007;26:385–389.
13. Mazzotta C, Balestrazzi A, Baiocchi S, Traversi C, Caporossi A. Stromal haze after combined riboflavin-UVA corneal collagen cross-linking in keratoconus: in vivo confocal microscopic evaluation. *Clin Exp Ophthalmol*. 2007;35:580–582.
14. Koppen C, Vryghem JC, Gobin L, Tassignon MJ. Keratitis and corneal scarring after UVA/riboflavin cross-linking for keratoconus. *J Refract Surg*. 2009;25:S819–S823.
15. Sharma A, Mohan K, Niranakari VS. Endothelial failure after collagen cross-linking with riboflavin and UV-A: case report with literature review. *Cornea*. 2013;32:e180–e181.
16. Wollensak G. Crosslinking treatment of progressive keratoconus: new hope. *Curr Opin Ophthalmol*. 2006;17:356–360.
17. Iseli HP, Thiel MA, Hafezi F, Kampmeier J, Seiler T. Ultraviolet A/riboflavin corneal cross-linking for infectious keratitis associated with corneal melts. *Cornea*. 2008;27:590–594.
18. Moren H, Malmsjo M, Mortensen J, Ohrstrom A. Riboflavin and ultraviolet a collagen crosslinking of the cornea for the treatment of keratitis. *Cornea*. 2010;29:102–104.
19. Cherfan D, Verter EE, Melki S, et al. Collagen cross-linking using rose Bengal and green light to increase corneal stiffness. *Invest Ophthalmol Vis Sci*. 2013;54:3426–3433.
20. Bak-Nielsen S, Pedersen IB, Ivarsen A, Hjortdal J. Dynamic Scheimpflug-based assessment of keratoconus and the effects of corneal cross-linking. *J Refract Surg*. 2014;30:408–414.
21. Ortiz D, Pinero D, Shabayek MH, Arnalich-Montiel F, Alio JL. Corneal biomechanical properties in normal, post-laser in situ keratomileusis, and keratoconic eyes. *J Cataract Refract Surg*. 2007;33:1371–1375.
22. Shah S, Laiquzzaman M, Bhojwani R, Mantry S, Cunliffe I. Assessment of the biomechanical properties of the cornea with the ocular response analyzer in normal and keratoconic eyes. *Invest Ophthalmol Vis Sci*. 2007;48:3026–3031.
23. Gkika M, Labiris G, Giarmoukakis A, Koutsogianni A, Kozobolis V. Evaluation of corneal hysteresis and corneal resistance factor after corneal cross-linking for keratoconus. *Graefes Arch Clin Exp Ophthalmol*. 2012;250:565–573.
24. Greenstein SA, Fry KL, Hersh PS. In vivo biomechanical changes after corneal collagen cross-linking for keratoconus and corneal ectasia: 1-year analysis of a randomized, controlled, clinical trial. *Cornea*. 2012;31:21–25.
25. Goldich Y, Barkana Y, Morad Y, Hartstein M, Avni I, Zadok D. Can we measure corneal biomechanical changes after collagen cross-linking in eyes with keratoconus?–a pilot study. *Cornea*. 2009;28:498–502.
26. Wollensak G, Spoerl E, Seiler T. Stress-strain measurements of human and porcine corneas after riboflavin-ultraviolet-A-induced cross-linking. *J Cataract Refract Surg*. 2003;29:1780–1785.
27. Kling S, Remon L, Perez-Escudero A, Merayo-Lloves J, Marcos S. Corneal biomechanical changes after collagen cross-linking from porcine eye inflation experiments. *Invest Ophthalmol Vis Sci*. 2010;51:3961–3968.
28. Palko JR, Tang JH, Perez BC, Pan XL, Liu J. Spatially heterogeneous corneal mechanical responses before and after riboflavin-ultraviolet-A crosslinking. *J Cataract Refract Surg*. 2014;40:1021–1031.
29. Nguyen TM, Aubry JF, Touboul D, et al. Monitoring of cornea elastic properties changes during UV-A/riboflavin-induced

corneal collagen cross-linking using supersonic shear wave imaging: a pilot study. *Invest Ophthalmol Vis Sci*. 2012;53:5948–5954.

30. Vaughan JM, Randall JT. Brillouin scattering, density and elastic properties of the lens and cornea of the eye. *Nature*. 1980;284:489–491.
31. Scarcelli G, Pineda R, Yun SH. Brillouin optical microscopy for corneal biomechanics. *Invest Ophthalmol Vis Sci*. 2012;53:185–190.
32. Scarcelli G, Yun SH. In vivo Brillouin optical microscopy of the human eye. *Opt Express*. 2012;20:9197–9202.
33. Scarcelli G, Besner S, Pineda R, Yun SH. Biomechanical characterization of keratoconus corneas ex vivo with Brillouin microscopy. *Invest Ophthalmol Vis Sci*. 2014;55:4490–4495.
34. Scarcelli G, Kling S, Quijano E, Pineda R, Marcos S, Yun SH. Brillouin microscopy of collagen crosslinking: noncontact depth-dependent analysis of corneal elastic modulus. *Invest Ophthalmol Vis Sci*. 2013;54:1418–1425.
35. Redhu N, Rastogi D, Yadav A, et al. Ultrasound elastography—review. *Curr Med Res Pract*. 2015;5:67–71.
36. Ophir J, Cespedes I, Ponnekanti H, Yazdi Y, Li X. Elastography: a quantitative method for imaging the elasticity of biological tissues. *Ultrason Imaging*. 1991;13:111–134.
37. Mariappan YK, Glaser KJ, Ehman RL. Magnetic resonance elastography: a review. *Clin Anat*. 2010;23:497–511.
38. Muthupillai R, Lomas DJ, Rossman PJ, Greenleaf JF, Manduca A, Ehman RL. Magnetic resonance elastography by direct visualization of propagating acoustic strain waves. *Science*. 1995;269:1854–1857.
39. Venkatesh SK, Yin M, Ehman RL. Magnetic resonance elastography of liver: technique, analysis, and clinical applications. *J Magn Reson Imaging*. 2013;37:544–555.
40. Itoh A, Ueno E, Tohno E, et al. Breast disease: clinical application of US elastography for diagnosis. *Radiology*. 2006;239:341–350.
41. Huang D, Swanson EA, Lin CP, et al. Optical coherence tomography. *Science*. 1991;254:1178–1181.
42. Schmitt J. OCT elastography: imaging microscopic deformation and strain of tissue. *Opt Express*. 1998;3:199–211.
43. Wang S, Larin KV. Optical coherence elastography for tissue characterization: a review. *J Biophotonics*. 2015;8:279–302.
44. Sticker M, Hitzenberger CK, Leitgeb R, Fercher AF. Quantitative differential phase measurement and imaging in transparent and turbid media by optical coherence tomography. *Opt Lett*. 2001;26:518–520.
45. Li C, Guan G, Huang Z, Johnstone M, Wang RK. Noncontact all-optical measurement of corneal elasticity. *Opt Lett*. 2012;37:1625–1627.
46. Li J, Han Z, Singh M, Twa MD, Larin KV. Differentiating untreated and cross-linked porcine corneas of the same measured stiffness with optical coherence elastography. *J Biomed Opt*. 2014;19:110502.
47. Wang S, Larin KV. Shear wave imaging optical coherence tomography (SWI-OCT) for ocular tissue biomechanics. *Opt Lett*. 2014;39:41–44.
48. Han Z, Li J, Singh M, et al. Analysis of the effects of curvature and thickness on elastic wave velocity in cornea-like structures by finite element modeling and optical coherence elastography. *Appl Phys Lett*. 2015;106:233702.
49. Han Z, Aglyamov SR, Li J, et al. Quantitative assessment of corneal viscoelasticity using optical coherence elastography and a modified Rayleigh-Lamb equation. *J Biomed Opt*. 2015;20:20501.
50. Wang S, Larin KV. Noncontact depth-resolved micro-scale optical coherence elastography of the cornea. *Biomed Opt Express*. 2014;5:3807–3821.
51. Wang S, Larin KV, Li JS, et al. A focused air-pulse system for optical-coherence-tomography-based measurements of tissue elasticity. *Laser Phys Lett*. 2013;10:075605.
52. Li J, Han Z, Singh M, Twa MD, Larin KV. Differentiating untreated and cross-linked porcine corneas of the same measured stiffness with optical coherence elastography. *J Biomed Opt*. 2014;19:110502.
53. Manapuram RK, Manne VGR, Larin KV. Development of phase-stabilized swept-source OCT for the ultrasensitive quantification of microbubbles. *Laser Phys*. 2008;18:1080–1086.
54. Manapuram RK, Manne VGR, Larin KV. Phase-sensitive swept source optical coherence tomography for imaging and quantifying of microbubbles in clear and scattering media. *J Appl Phys*. 2009;105:102040.
55. Liu J, He X. Corneal stiffness affects IOP elevation during rapid volume change in the eye. *Invest Ophthalmol Vis Sci*. 2009;50:2224–2229.
56. Manapuram RK, Aglyamov S, Menodiado FM, et al. Estimation of shear wave velocity in gelatin phantoms utilizing PhS-SSOCT. *Laser Phys*. 2012;22:1439–1444.
57. Song S, Huang Z, Wang RK. Tracking mechanical wave propagation within tissue using phase-sensitive optical coherence tomography: motion artifact and its compensation. *J Biomed Opt*. 2013;18:121505.
58. Mandell RB. Corneal power correction factor for photorefractive keratectomy. *J Refract Corneal Surg*. 1993;10:125–128.
59. Graff KF. *Wave Motion in Elastic Solids*. New York: Courier Corporation; 1975.
60. Singh M, Wu C, Liu CH, et al. Phase-sensitive optical coherence elastography at 1.5 million A-Lines per second. *Opt Lett*. 2015;40:2588–2591.
61. Kirk RW, Kennedy BF, Sampson DD, McLaughlin RA. Near video-rate optical coherence elastography by acceleration with a graphics processing unit. *J Lightwave Technol*. 2015;33:3481–3485.
62. Drexler W, Liu M, Kumar A, Kamali T, Unterhuber A, Leitgeb RA. Optical coherence tomography today: speed, contrast, and multimodality. *J Biomed Opt*. 2014;19:071412.
63. Fechtig DJ, Grajciar B, Schmoll T, et al. Line-field parallel swept source MHz OCT for structural and functional retinal imaging. *Biomed Opt Express*. 2015;6:716–735.
64. Wieser W, Biedermann BR, Klein T, Eigenwillig CM, Huber R, Multi-megahertz OCT: high quality 3D imaging at 20 million A-scans and 4.5 GVoxels per second. *Opt Express*. 2010;18:14685–14704.
65. Torricelli AA, Ford MR, Singh V, Santhiago MR, Dupps WJ Jr, Wilson SE. BAC-EDTA transepithelial riboflavin-UVA cross-linking has greater biomechanical stiffening effect than standard epithelium-off in rabbit corneas. *Exp Eye Res*. 2014;125:114–117.
66. Dorronsoro C, Pascual D, Perez-Merino P, Kling S, Marcos S. Dynamic OCT measurement of corneal deformation by an air puff in normal and cross-linked corneas. *Biomed Opt Express*. 2012;3:473–487.
67. Ford MR, Sinha Roy A, Rollins AM, Dupps WJ Jr. Serial biomechanical comparison of edematous, normal, and collagen crosslinked human donor corneas using optical coherence elastography. *J Cataract Refract Surg*. 2014;40:1041–1047.
68. Liu J, Roberts CJ. Influence of corneal biomechanical properties on intraocular pressure measurement: quantitative analysis. *J Cataract Refract Surg*. 2005;31:146–155.
69. Medeiros FA, Weinreb RN. Evaluation of the influence of corneal biomechanical properties on intraocular pressure measurements using the ocular response analyzer. *J Glaucoma*. 2006;15:364–370.

Investigative Ophthalmology & Visual Science

70. Hoeltzel DA, Altman P, Buzard K, Choe K. Strip extensiometry for comparison of the mechanical response of bovine, rabbit, and human corneas. *J Biomech Eng*. 1992;114:202–215.
71. Seiler T, Hafezi F. Corneal cross-linking-induced stromal demarcation line. *Cornea*. 2006;25:1057–1059.
72. Han Z, Li J, Singh M, et al. Quantitative methods for reconstructing tissue biomechanical properties in optical coherence elastography: a comparison study. *Phys Med Biol*. 2015;60:3531–3547.
73. Elsheikh A, Alhasso D. Mechanical anisotropy of porcine cornea and correlation with stromal microstructure. *Exp Eye Res*. 2009;88:1084–1091.
74. Elsheikh A, Brown M, Alhasso D, Rama P, Campanelli M, Garway-Heath D. Experimental assessment of corneal anisotropy. *J Refract Surg*. 2008;24:178–187.
75. Nguyen TM, Aubry JF, Fink M, Bercoff J, Tanter M. In vivo evidence of porcine cornea anisotropy using supersonic shear wave imaging. *Invest Ophthalmol Vis Sci*. 2014;55:7545–7552.
76. Pinsky PM, van der Heide D, Chernyak D. Computational modeling of mechanical anisotropy in the cornea and sclera. *J Cataract Refract Surg*. 2005;31:136–145.
77. Li J, Wang S, Singh M, et al. Air-pulse OCE for assessment of age-related changes in mouse cornea in vivo. *Laser Phys Lett*. 2014;11:065601.
78. Geraghty B, Whitford C, Boote C, Akhtar R, Elsheikh A. *Age-Related Variation in the Biomechanical and Structural Properties of the Corneo-Scleral Tunic. Mechanical Properties of Aging Soft Tissues*. Cham, Switzerland: Springer; 2015;207–235.

Investigative Ophthalmology & Visual Science